Fundamental study of a single point lean direct injector. Part I: effect of air swirler angle and injector tip location on spray characteristics

Sarah A. Tedder[1], Yolanda R. Hicks[2], Kathleen M. Tacina [3] and Robert C. Anderson [4]
NASA Glenn Research Center, Cleveland, Ohio 44135

Lean direct injection (LDI) is a combustion concept to reduce oxides of nitrogen (NO_x) for next generation aircraft gas turbine engines. These newer engines have cycles that increase fuel efficiency through increased operating pressures, which increase combustor inlet temperatures. NO_x formation rates increase with higher temperatures; the LDI strategy avoids high temperature by staying fuel lean and away from stoichiometric burning. Thus, LDI relies on rapid and uniform fuel/air mixing. To understand this mixing process, a series of fundamental experiments are underway in the Combustion and Dynamics Facility at NASA Glenn Research Center. This first set of experiments examines cold flow (non-combusting) mixing using air and water. Using laser diagnostics, the effects of air swirler angle and injector tip location on the spray distribution, recirculation zone, and droplet size distribution are examined. Of the three swirler angles examined, 60º is determined to have the most even spray distribution. The injector tip location primarily shifts the flow without changing the structure, unless the flow includes a recirculation zone. When a recirculation zone is present, minimum axial velocity decreases as the injector tip moves downstream towards the venturi exit; also the droplets become more uniform in size and angular distribution.

Nomenclature

CFD	=	computational fluid dynamics
D_t	=	venturi throat diameter
FN_{US}	=	injector flow number
h	=	distance upstream of venturi throat
LDI	=	lean direct injection, lean direct injector
PIV	=	particle image velocimetry
PLS	=	planar laser scatter
r	=	distance from LDI exit
S	=	swirl number
SV	=	swirler venturi

I. Introduction

For more than 40 years, NASA has sustained programs to reduce the environmental effects of aviation. A major focus of these programs has been reducing the emissions of nitrogen oxides (NO_x). NO_x emissions decrease the protective ozone layer in the stratosphere and increase smog and ozone in the lower troposphere[1]. To prevent damage to the protective ozone layer, NASA programs have focused on reducing NO_x at cruise for supersonic flight. To reduce the emissions of NO_x in the lower troposphere, NASA programs have also focused on reducing NO_x emissions during the landing-takeoff cycle in subsonic flight.

In addition to decreasing NO_x emissions, NASA has also addressed the reduction of carbon dioxide emissions by

[1] Researcher, Combustion Branch, MS 5-10, and AIAA Non-Member.
[2] Researcher, Combustion Branch, MS 5-10, and AIAA Non-Member.
[3] Researcher, Combustion Branch, MS 5-10, and AIAA Non-Member.
[4] Researcher, Optics and Photonics Branch, MS 77-1 and AIAA Non-Member.

increasing engine fuel efficiency. Increased fuel efficiency is typically achieved by increasing the engine operating pressure ratio, which increases combustor inlet temperature; however, NO_x formation rates increase with higher temperatures. Without an improvement in combustor technology, higher efficiency engines will have higher, not lower, NO_x emissions. Therefore, improved low-NO_x combustor technologies need to be developed.

In order to reduce NO_x emissions, NASA is exploring fuel-lean front-end concepts. Historically, turbine engines for aircraft use rich-front-end combustors in order to ensure stable combustion in flight. In these combustors the primary combustion zone is fuel-rich — only part of the combustion air enters through the fuel/air mixers; the rest enters through downstream dilution jets, allowing combustion to be completed[2,3,4]. In contrast, lean-front-end combustors operate fuel-lean throughout: All of the combustor air except that used for liner cooling enters through the combustor dome. Lean front end combustion concepts include lean, premixed, prevaporized (LPP), lean partially premixed, and lean direct injection (LDI) combustion[2,5,6,7,8,9]. This paper focuses on an LDI combustion concept.

LDI and other lean front end combustion concepts minimize local flame temperature. This keeps NO_x emissions low because NO_x is an exponential function of local temperature. To minimize NO_x emissions, fuel-lean combustion needs to avoid local near-stoichiometric zones where the flame temperature is high. Avoiding these zones requires rapid and uniform fuel/air mixing. LDI accomplishes this mixing in part by replacing one traditionally-sized fuel/air mixer with multiple smaller fuel/air mixers. However, previous experiments have shown that decreasing the size and increasing the number of fuel/air mixers alone does not sufficiently improve mixing: fuel/air mixer design is also important.

Multiple fuel/air mixer designs have been studied. There are several ways an individual fuel/air mixer can be constructed. On the air side, a radial, axial, or discrete jet swirler may be used. With any of these types of swirlers, the swirl number can be varied. A venturi can be placed downstream of the air swirler, or the venturi can be omitted. On the fuel side, a simplex or air assist-atomizer can be used. For a simplex atomizer, flow number (i.e., effective flow area) can be varied. In addition, once a fuel/air mixer design has been chosen, the size and number of the mixer elements can be varied.

In order to choose the best fuel/air mixer design for an LDI combustor, it is critical to understand the fuel/air mixing process. Understanding fuel/air mixing requires knowledge both of large overall features such as recirculation zones and precessing vortices, and of smaller eddies where much of the mixing occurs. To better understand the mixing process, the NASA Fundamental Aeronautics/Aeronautical Sciences project is conducting a series of tests in the 5-atm Combustion and Dynamics Facility (CDF) flametube rig at NASA Glenn Research Center.

The baseline swirl-venturi (SV) LDI fuel/air mixer[2,6] was used for these studies. The baseline SV-LDI fuel/air mixer consists of an axial swirler followed by a venturi. Fuel is injected through a simplex fuel injector; the fuel injector tip is at or just upstream of the venturi throat.

This first set of experiments examines cold flow mixing using water. It studies the effect of air swirler angle and fuel injector tip location on the cold flow droplet size and velocity fields. Testing was done at a temperature of 700 K and a pressure of 517-kPa. Water was used in place of jet fuel to prevent auto-ignition during long run times. Diagnostic measurements included particle image velocimetry, 30 kHz high-speed video images of planar laser scatter, and shadowgraph images for droplet size measurement. The results from these measurements are used to examine the effects of air swirler angle and injector tip location on the spray distribution, recirculation zone, and droplet size distribution.

II. Experimental Facilities and Hardware

A. Combustion and Dynamic Facility (CDF)

All testing was done at NASA Glenn Research Center in the Combustion and Dynamics Facility (CDF). A schematic of the CDF test rig is shown in Fig. 1. The CDF is orientated vertically, with the flow going down. The CDF can supply non-vitiated air preheated up to 810 K at air flow rates up to 0.35 kg/sec and pressures up to 517-kPa. The combustor test section has a circular cross-section nominally 7.62-cm in diameter. Three sets of double-paned windows, spaced 90° apart around its circumference, are used to gain optical access to the water-cooled combustor. The two opposing windows are aligned to provide access in the x direction, while the third window is on the –y side of the combustor. The windows are flat and have a small offset away from the combustor circumference. The windows measure 6.1-cm tall (axial direction) by 5.8-cm wide (azimuthal). Fig. 2 shows a cross sectional detail drawing of the combustor, which defines the coordinate system and shows the window positions.

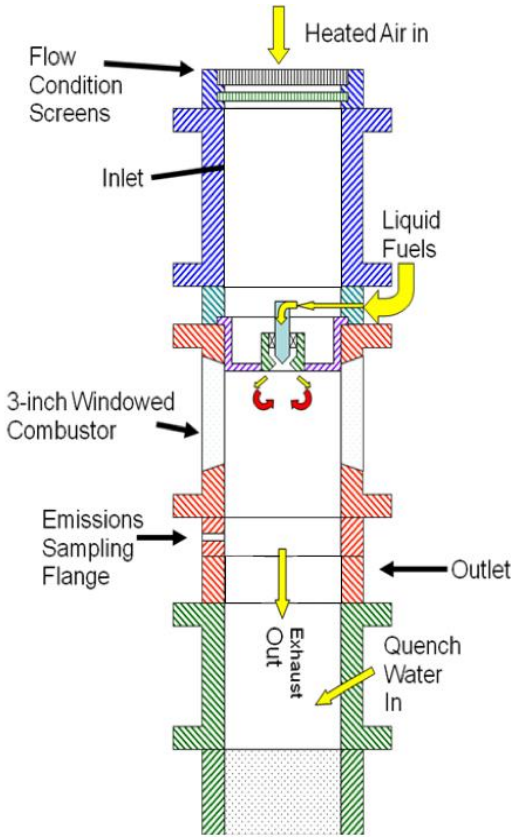

Figure 1. Schematic of the test hardware. *This schematic is not to scale.*

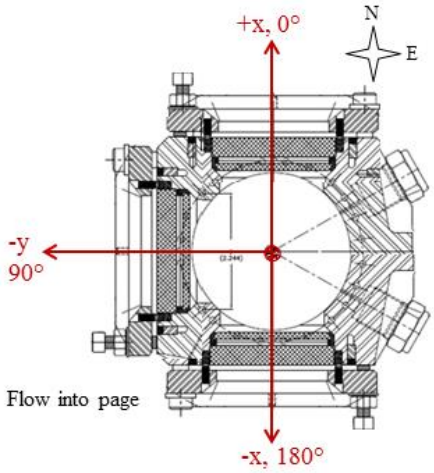

Figure 2. Cross sectional detail of combustor. *Shown by red arrows are the window orientation and definition of the coordinate system used. Z is into the page.*

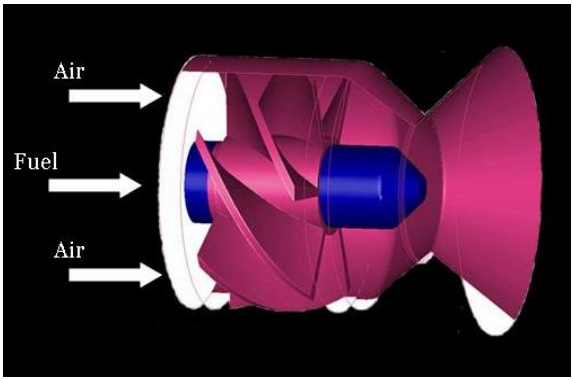

Figure 3. Schematic drawing of a single SV-LDI fuel/air mixer.

B. LDI Hardware

As illustrated in Fig. 3 and 4, the baseline SV-LDI fuel/air mixer consists of a simplex pressure-swirl fuel injector and an air passage with a six-bladed, helical axial air swirler followed by a converging-diverging venturi section. The diameter of the venturi throat (D_t) is 13.0 mm. The simplex fuel injector is inserted through the center of the air swirler. The fuel injector

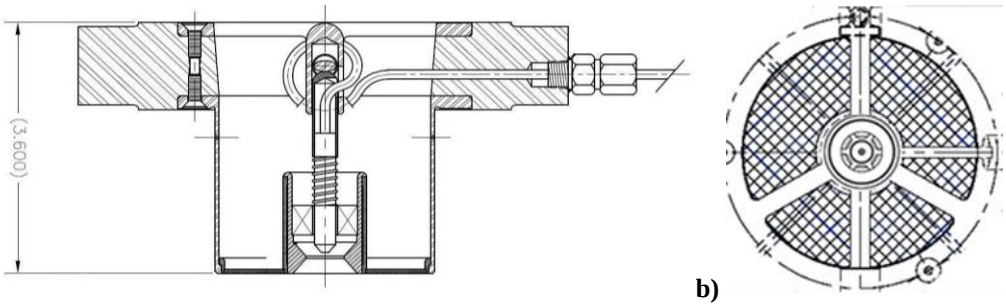

a) **b)**

Figure 4. Cross section of the single SV-LDI module. *Detailed drawings showing a cross section of the single SV-LDI module in its spool piece; (a) and a bottom view that shows the screen inserted around the module (b).*

tip is placed at one of three distances upstream of the venturi throat, h/D_t: 0, 0.16, or 0.31 throat diameters. The injector flow number, $FN_{US,}$ (as defined by Lefebvre[10]) is 0.7. The helical axial air swirlers have six blades. Each blade has an inside diameter of 9.4 mm and an outside diameter of 22 mm. The blades angles for three configurations studied here are 45°, 52.5°, and 60°. The calculated swirl numbers, as defined by Beer and Chigier[11], are 0.59, 0.77, and 1.02, respectively.

This baseline SV-LDI fuel/air mixer is nominally 2.54-cm in diameter. However, the flametube is 7.62-cm in diameter. In this study, the fuel/air mixer was mounted in the center of the flametube and surrounded by co-flow air; the co-flow enters the flametube through a screen that simulates the pressure drop across the fuel/air mixer. The test hardware is shown in Fig. 4.

C. Test Conditions

Results from two test conditions are presented in the results and discussion section. These test conditions will be referred to as test points 500 and 700. These conditions are detailed in Table 1. The combustor air inlet temperature and pressure were the same for both test points 700 K and 517 kPa. The test point 500 has a lower reference velocity and a higher water to air ratio than the 700 test point. The water was injected at the same ambient temperature (~298 K) for both test conditions.

Table 1. Test Conditions. *Common conditions for both test points, 500 and 700: Air: Pressure=517.1 kPa, Temperature = 700 K. The water was at room temperature, approximately 298K.*

Test Point	Reference Velocity (m/s)	Air Flow Rate (kg/s)	Water Flow Rate (kg/h)	Water/Air Ratio	$\Delta P_{injector}$ (kPa)
500	9.1	0.107	3.89	0.100	672
700	12.2	0.143	4.09	0.008	738

D. Optical Instrumentation

For the work presented here, we measured water droplet velocities and sizes in preheated air. Two-dimensional velocity measurements were obtained using particle image velocimetry (PIV). The shadowgraph technique was used to obtain drop sizes and instantaneous velocity measurements of water spray. Planar laser scatter (PLS) was used to visualize liquid drops at a high frame rate and to develop limited pseudo time-series PIV. High frame rate PLS images were also used to develop spray pattern histograms. All techniques were laser-based. The lasers were located in a separate room and the light was transmitted to the test rig using mirrors, and then conditioned to the appropriate measurement volume via combinations of lenses. The details of the experimental setups are outlined below.

Standard PIV and PLS, used similar optical arrangements. The laser light for PIV and PLS entered and exited the combustor in the x-direction via the two opposing windows at 0° and 180°, and the camera, which received the 90°-scattered light was positioned to collect the light via the window at 90°. For shadowgraphy, a line-of-sight technique, the light source and camera were positioned on opposite sides, using the two opposing windows.

PIV data were obtained using a dual head, frequency-doubled Nd:YAG laser operating at 15 Hz. The laser pulse width was 3-5 ns. The spatially-overlapped laser beams were expanded into vertically-oriented sheets using a cylindrical lens. The sheets were approximately 45-mm-high by 0.3-mm thick, entered the combustor through the 180° window, and exited through the 0° window. The sheet axis was aligned with the flow direction. Images were acquired through the 90° window, collecting light scattered from water droplets that passed through the laser sheet, to capture liquid phase velocity. To collect the light, we used an f = 105-mm, f/4 lens, outfitted with a 532-nm narrowband interference filter. An interline transfer CCD camera (1600 x 1200 pixels) captured the scattered light from adjacent laser pulses onto two individual frames. This collection scheme imaged a region that spanned roughly 50-mm in the x-direction (along the laser sheet axis) by 38-mm axially (z-direction). The time between frames was typically 5 μs. All synchronization was handled using a LaVision, Inc. programmable timing unit, PTU-9. Cross-correlation methods were then applied to create a displacement vector field for each image pair. LaVision's DaVis software version 7.2 was used to collect the images and version 8.2 was used to produce 2-D fields of the axial-horizontal (z-x) velocity components in the y = 0 plane.

Shadowgraph images were produced using the same laser and camera. However, for the shadowgraph measurements the laser was expanded into a cone using a spherical lens, which in turn struck a fluorescent plate,

producing a bright, yellow-orange background field. Light was collected on the opposite side with a long-range catadioptric microscope and stored on the camera. The system magnification was such that each image provided a field of view of approximately 2.2-mm in the y-direction, by 1.7-mm high (z-direction), with a depth of field of approximately 1-mm. Each image was considered to emanate from a "point" in space, and the whole optical system was traversed in 1- or 2-mm increments in the x-direction, along y = 0, with occasional data collected along x = 0.

PLS images were acquired using a continuous wave Nd:YAG laser with a total power output of ~1.1 watts. As with PIV, the laser beam was formed into a vertical sheet (approximately 40-mm high, positioned along y = 0). The laser sheet entered via the 0° window and exited through the 180° window. We used a 12-bit, grayscale, high-speed camera that has a CMOS array with 1024 x 1024 pixel resolution. The high-speed camera was set up square to the rig and focused on the vertical plane at y = 0. The high-speed camera frame rate and resolution are variable. The camera can frame as fast as 5400-frames/s (5.4-kps) at full resolution (which provides the maximum field-of view image size), and faster at lower resolutions. A frame rate of 30-kps and a resolution of 512 x 352 pixels was used. The light was collected using an f = 60-mm, f/2.8 lens. The default exposure is 1/(frame rate), or 33.3 µs, which was used for all PLS images.

III. Results and Discussion

The effects of air swirler angle and injector tip location on the velocity field and droplet size distribution are presented in this section. First, we discuss effects of the air swirler angle on the spray distribution, droplet size, and recirculation zone. We then discuss the injector tip location effect on spray distribution, droplet size, and recirculation zone.

A. Air Swirler Angle

This subsection examines the effect of air swirler angle when the injector tip is located at the venturi throat.

1. Spray Distribution

An even distribution of droplets in the injector spray improves the mixing of fuel and oxidizer, reducing production of NO_x by minimizing the occurrence of pockets of increased temperature caused by local peaks in fuel air ratio. One important parameter used to characterize the droplet distribution is the spray angle.

The spray angles can be observed qualitatively by examining the measured PIV velocity fields. Shown in Fig. 5 a), b), and c) are PIV velocity fields at y = 0, at test condition 500, with the injector tip at the venturi throat. These results indicate qualitatively that the spray angle of the droplets increases with increasing swirler angle.

We also measured the spray pattern using the high-speed images of PLS. For each condition we analyzed 1000 high-speed image frames using IDL[12] and software[13] which finds and measures roughly circular features within an image. For each of the features, a distance, r, and angle relative to the vertical measured from (x, y, z) = (0,0,0) were determined. Spray pattern histograms were developed by creating software "bins" which were 3° wide with an r that ranged from 10 to 30 mm. The software counted the features found in each bin throughout the 1000 frames analyzed. Results of this analysis are shown in Fig. 6, where all three plots are shown with the same scale. These histograms clearly indicate that the spray was a hollow cone, as expected from a simplex fuel injector. They also indicate that the number of droplets found in the center of the hollow cone increases with increasing swirler angle.

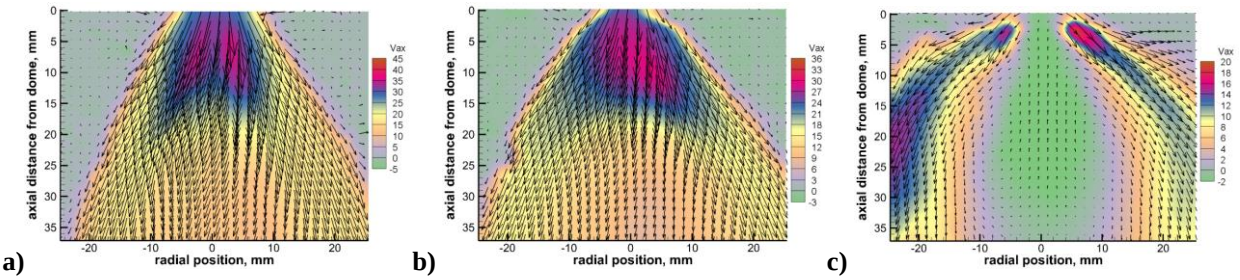

Figure 5. Average Velocity Fields. *Average velocity fields at y = 0 for water spray measured with PIV measured at test condition 500 with injector tip at the venturi throat. Increasing air swirler angle from left to right: (a) 45 degrees, (b) 52.5 degrees, (c) 60 degrees. The flow is from top to bottom.*

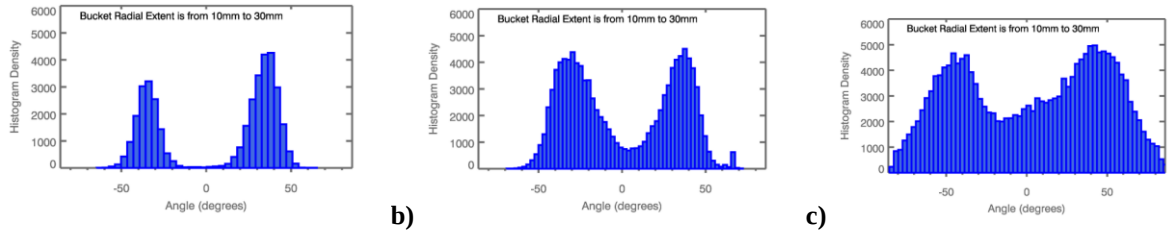

Figure 6. Histograms of Droplet Distributions. *Occurrences of droplets at angles relative to center of air mixer exit at test condition 500 with injector tip at the venturi throat. Increasing air swirler angle from left to right: (a) 45º, (b)52.5º, (c) 60º.*

Using the droplet distribution histograms, we define the spray angle as the difference between the bin angle where the total count reached 5% and the angle where the count reached 95%. These calculated spray angles are plotted versus swirler angle in Fig. 7. The trend in Fig. 7 closely matches the trends observed in the PIV velocity field in Fig. 5 (increasing spray angle with increasing swirler angle). In addition, in Fig. 7, one can note that the spray angle is higher at point 500 than at point 700 for swirler angles of 45º and 52.5º, but not for 60º.

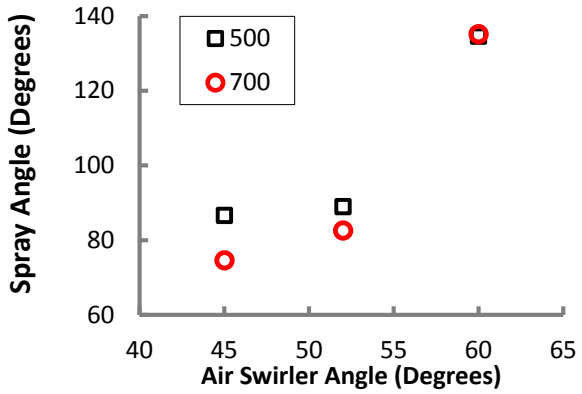

Figure 7. Effect of Air Swirler Angle on Spray angle. *Spray angle distribution versus Air swirler angle at test conditions 500 and 700. The injector tip is at the venturi throat.*

2. Droplet Size

The Sauter mean diameter (SMD) is plotted versus radial position for each swirler angle in Fig. 8. These measurements were collected at test point 500 with the injector tip at the throat. The SMD is measured at points along a line perpendicular to the flow at an axial location, z = 11 mm, downstream of venturi exit. The droplet size distribution is similar for swirler angles 45º and 52.5º with smaller droplets occurring towards the center of the spray and larger droplets near the outer edges. For these swirler angles the SMD ranges from 80 µm to below 20 µm. For swirler angle 60º, the size distribution is narrower, spanning from 30 µm to 60 µm across the scan. This may be a result of the presence of the recirculation zone produced by the 60º swirler angle as discussed in the next section.

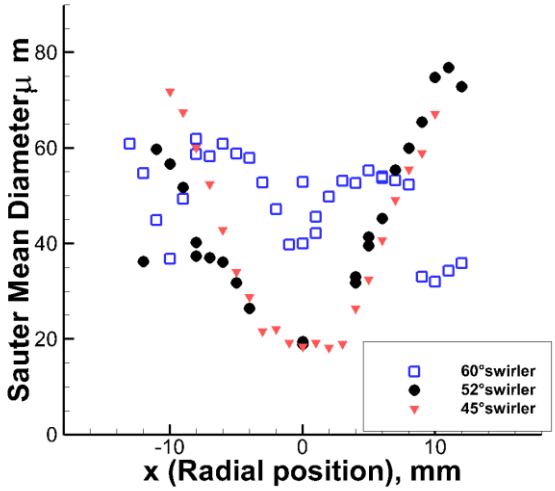

Figure 8. Sauter Mean Diameter versus Radial Position. *Plot of droplet diameter versus radial location, x, for test condition 500 with the injector tip at the throat of the venturi.*

3. Recirculation Zone

In gas turbine combustors, swirl is used to improve fuel/air mixing and to mix the combustion products with the unburned fuel and air, thereby decreasing flame length and increasing flame stability. Usually, the swirl is strong enough to cause reverse flow and a central recirculation zone forms downstream of the fuel/air mixer[10]. Previous work on swirling jets has shown that a central recirculation zone forms when the swirl number is greater than about 0.6[10,11,14]. Furthermore, a diverging flow passage has been shown to increase

the diameter and mass of fluid in the recirculation zone[11].

Since the SV-LDI geometry includes a converging-diverging venturi, a central recirculation zone would be expected as long as the swirl number was near 0.6. Therefore, the minimum swirler vane angle was chosen to be 45°, corresponding to a swirl number of 0.59[6]. However, subsequent optical diagnostic measurements[15] and CFD calculations[16] showed that with a swirler angle of 45° no central recirculation zone formed. This was true both for a single 2.54-cm SV-LDI fuel/air mixer in a 2.54-cm by 2.54-cm square duct[15,16] and an array of 3 by 3 fuel/air mixers in a 7.62-cm by 7.62-cm square duct[16]. In fact, the experiments conducted by Fu[15] on a single 2.54-cm SV-LDI in the 2.54-cm by 2.54-cm square duct showed that a strong central recirculation zone did not form until the swirler angle was well above 45°. In this experiment, Fu[15] varied the swirler angle from 40° to 65° in 5° increments. No central recirculation zone formed until the swirler angle was 55°; and even then, the central recirculation zone did extend to the venturi exit—it started about 22-mm downstream of the venturi exit. The central recirculation zone did not extend to the venturi exit until the swirler angle was 60°, S=1.02[15]. For a 3 by 3 array of fuel/air 60° swirler angle mixers, previous CFD calculations[16] and experimental measurements[17] also showed a recirculation zone extending to the venturi exit.

The experiment presented in this paper differs from these previous experiments[15,16,17] as it was done on a single 2.54-cm SV-LDI fuel/air mixer in a 7.62-cm circular duct. A single fuel/air mixer was studied to allow for detailed measurements to be taken without interaction from surrounding fuel/air mixers. However, this means that the boundary conditions, i.e., confinement, were significantly different than it would be in a more realistic case of seven 2.54-cm fuel/air mixers in the same 7.62-cm circular duct. Previous research[11,14,15,18] has shown that confinement can significantly affect the velocity field and recirculation zone. Therefore, to partially simulate the effects of multiple fuel/air mixers, a coflow was used. Although this experiment had a coflow whereas the previous research did not[16,17], the current results are consistent: a recirculation zone was observed for the 60° swirler but not for the 45° swirler. There was also no recirculation zone for the 52.5° swirler.

In this work the value and location of the minimum axial velocity for various swirler angles was used as an indicator of the effect swirler angle (shown in Fig. 9). This was done since the neither the 45° swirler nor the 52.5° swirler case produced a recirculation zone. Fig. 9 a) shows that the minimum axial velocity decreases with increasing swirler angle. In Fig. 9 b) for both the 45° swirler and the 52.5° swirler, the minimum axial velocity is at the downstream edge of the field of view, z≈36 mm; this means that the actual location of the minimum axial velocity may be farther downstream and that the minimum velocity may be lower. For the 60° swirler, the location of the minimum axial velocity (i.e., greatest reverse flow) is much farther upstream.

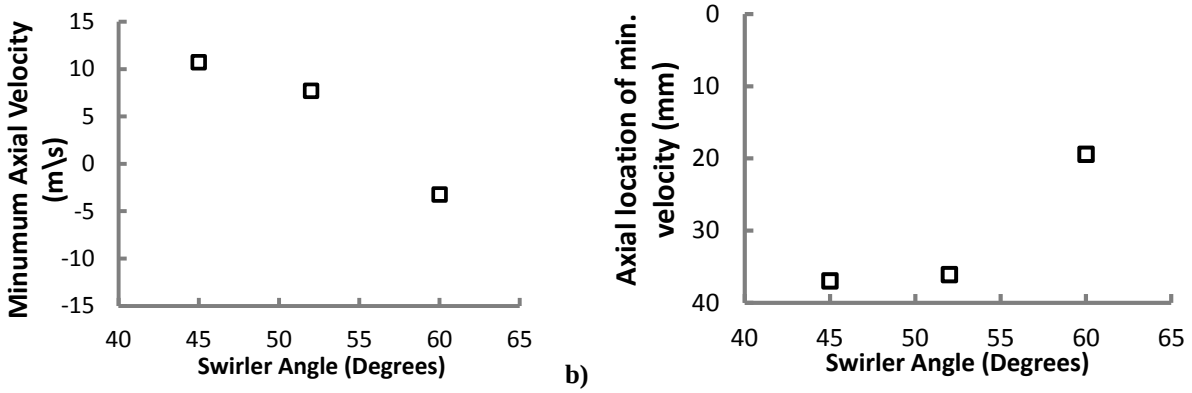

Figure 9. Effect of Swirler Angle on Minimum Axial Velocity. *The injector tip is at the venturi throat and test condition is 500. Shown are a) minimum axial velocity and b) axial location of this minimum axial velocity versus swirler angle.*

B. Injector Tip Location

This subsection examines the effect of the injector tip location on spray distribution and droplet size distribution for all three swirler angles, and the recirculation zone for the 60º swirler angle.

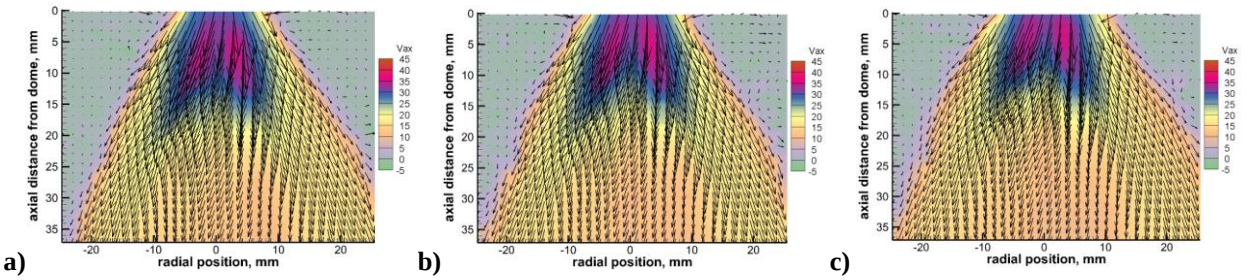

Figure 10. Average Velocity Fields, 45º swirler, Condition 500. *Average velocity fields for water spray measured with PIV at test condition 500 with 45º swirler angle. Injector tip distances upstream of the throat, h/D_t are a) 0, b) 0.16, and c) 0.31. The flow is from top to bottom.*

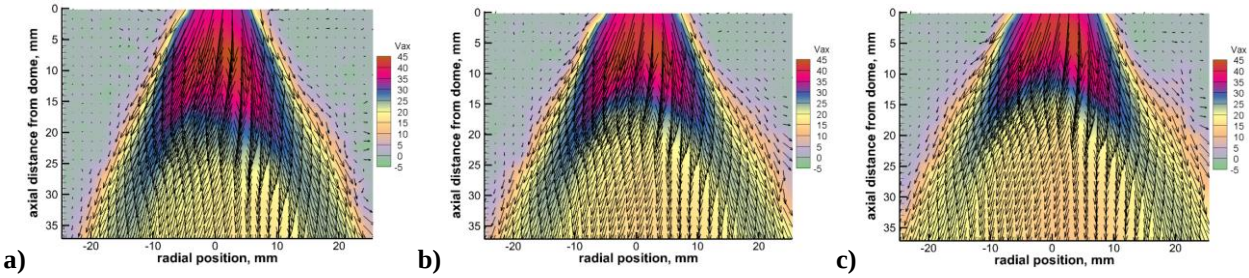

Figure 11. Average Velocity Fields, 45º swirler, Condition 700. *Average velocity fields for water spray measured with PIV at test condition 700 with 45º swirler angle. Injector tip distances upstream of the throat, h/D_t are a) 0, b) 0.16, and c) 0.31. The flow is from top to bottom.*

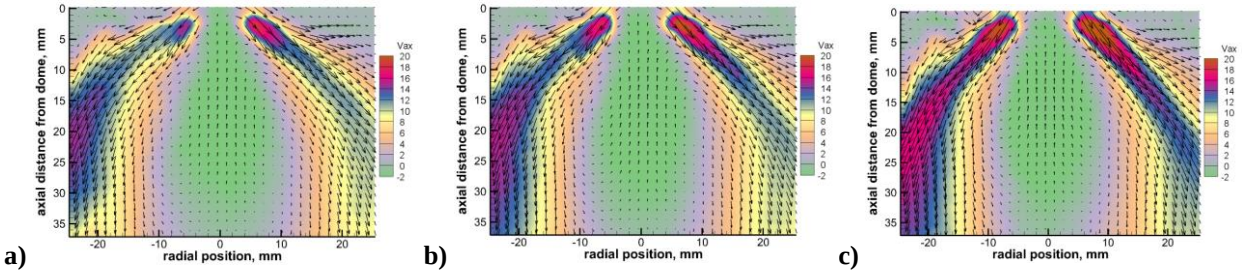

Figure 12. Average Velocity Fields, 60º swirler . *Average velocity fields for water spray measured with PIV at test condition 500 with 60º swirler angle. Injector tip distances upstream of the throat, h/D_t are a) 0, b) 0.16, and c) 0.31. The flow is from top to bottom.*

1. Spray Distribution

To examine the spray distribution, PIV results along the y = 0 combustor position are shown at both conditions 500 and 700 in Figs. 10 and 11 for swirler angle 45º, and in Fig. 12 at test condition 500 for swirler angle 60º. The flow is from top to bottom. From left to right in these figures, h/D_t is 0, -0.16, and -0.31. In Fig. 10 and 11, the results show that the spray angle increases as the injector tip is moved farther upstream of the throat. For the 60° swirler (Fig. 12), it is harder to discern by eye, but the trend appears to be opposite. A more quantitative consideration of the effect is shown in Fig. 13, which shows plots of spray angle versus injector tip location calculated from the histograms as described in the spray distribution section above. These graphs show agreement with the visual observations made for the PIV images, and emphasize that there is only a minor change of spray angle for the 60° air swirler with injector tip position (Fig. 13 c).

To understand the effect of the injector tip location further, the histograms from the 60º swirler are examined. Figure 14 a), b), and c) show histograms of the droplet distributions for the range of spray angles measured for test condition 700 with h/D_t of 0, -0.16, and - 0.31. The histograms show that the distribution becomes more uniform as the injector tip is moved closer to the throat.

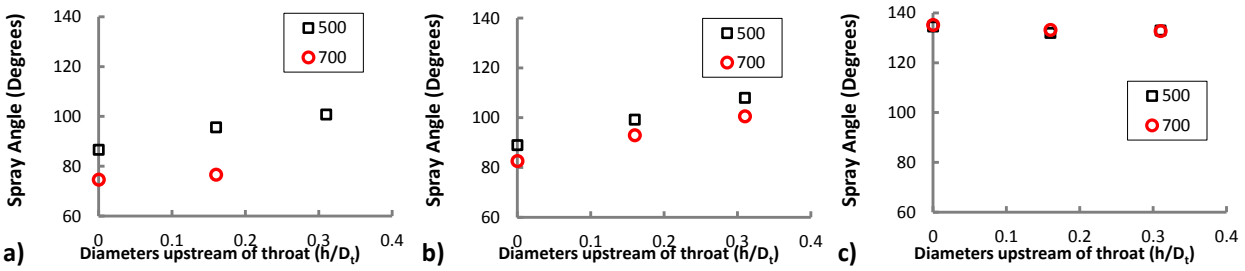

Figure 13. Effect of Injector Tip Location on Spray Angle. *Plots of spray angle versus location of injector tip diameter measured in h/D$_t$. From left to right the plots are for swirler angles 45º, 52.5º, and, 60º*

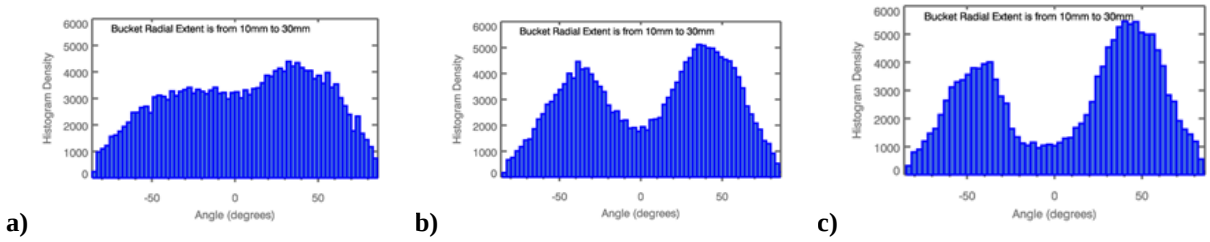

Figure 14. Histograms of Droplet Distributions of Swirler Angle 60º. *Occurrences of droplets at angles relative to center of air mixer exit at test condition 700 with injector tip at the venturi throat. Injector tip distance upstream of the throat in throat diameters: (a) at throat, (b)0.16, (c) 0.31.*

2. Droplet Size

Figure 15 shows the SMD for the various injector tip locations, measured across the flow at the axial location z = 11 mm (11 mm downstream of venturi exit). The plots show that as the injector tip moves downstream the droplet sizes are larger in the center region of the of the flow from ~ x= -10 mm to 10 mm. This is most evident for Fig. 15 a) for swirler angle 60º, test condition 700. This trend is also seen for Fig. 15 b) for swirler angle 52.5º, test condition 700. There are many possible reasons for increase in uniformity of the droplet sizes such as: a simple shift of the flow downstream or droplet coagulation. To determine the cause of these trends, droplets sizes need to be measured at several more axial locations.

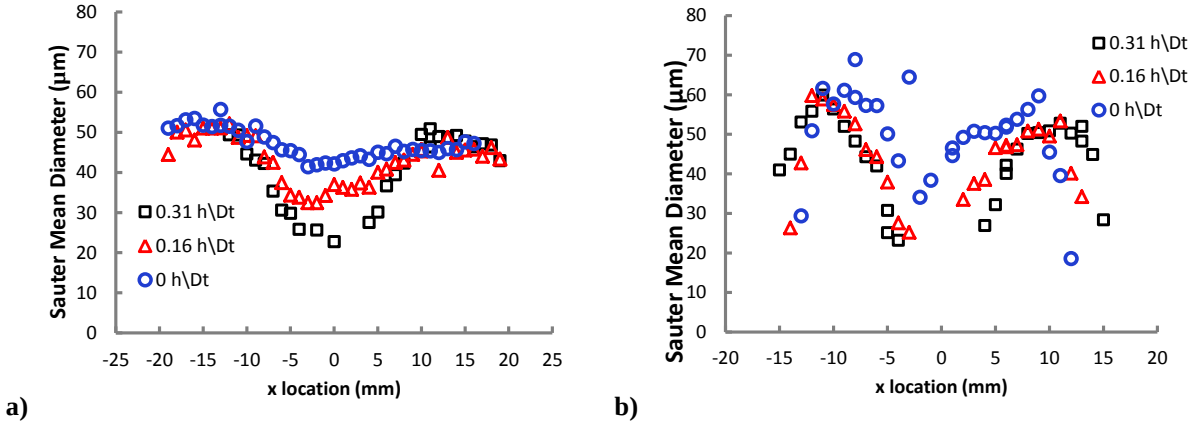

Figure 15. Droplet Size Distribution Effect of Injector Tip. *a) Plot of droplet size verses versus x (radial) location for a range of injector tip locations at test condition 700 and swirler angle 60º. b) Plot of droplet size versus radial location for a range of injector tip locations at test condition 700 and swirler angle 52.5º.*

3. Recirculation Zone

The recirculation zone generated using the 60° swirler was characterized based on its size and minimum velocity. The velocity field for the 60º swirler flow, as seen in Fig. 12, shows that the region measured with the PIV in this experiment does not include the stagnation point of the recirculation zone. The field of view only includes the top portion of the primary zone as shown in the drawing representation of the flow in Fig. 16. Because of this limited field of view, the outer bounds of the recirculation zone cannot be determined. Hence in order to measure the width of the recirculation zone, the zero velocity line is used instead. The maximum width of zero velocity area of the recirculation zone is plotted versus the injector tip location in Fig. 17 a). This plot shows that the recirculation zone has a width that is almost constant, but is slightly wider with the injector tip at the throat. The location of this maximum width plotted versus the location of the

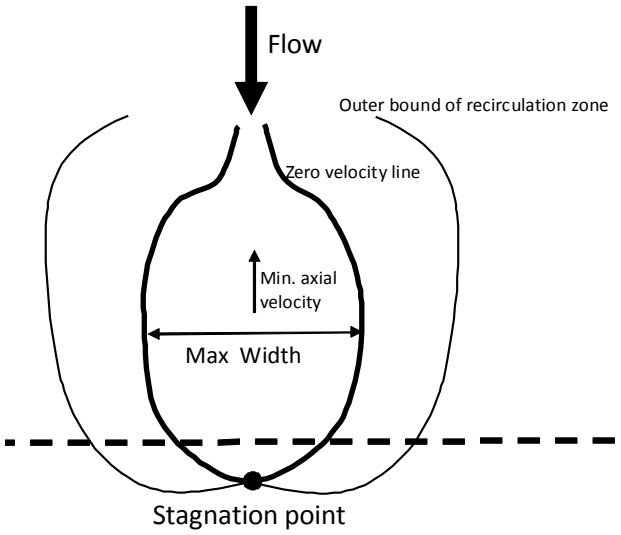

Figure 16. Drawing of the Recirculation Zone. *Drawing of the flow with a recirculation zone. The field of view for this experiment only include the area above the dashed line.*

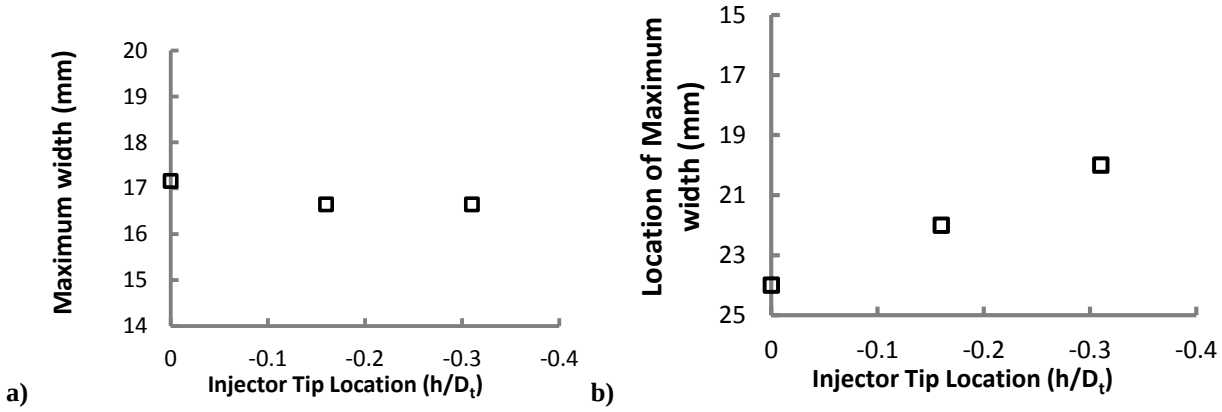

Figure 17. Measures of Recirculation Zone Size. *a) Plot of maximum width versus injector tip location diameter upstream of throat. b) Plot of location of maximum width versus injector tip location. Swirler angle 60º and test condition 500.*

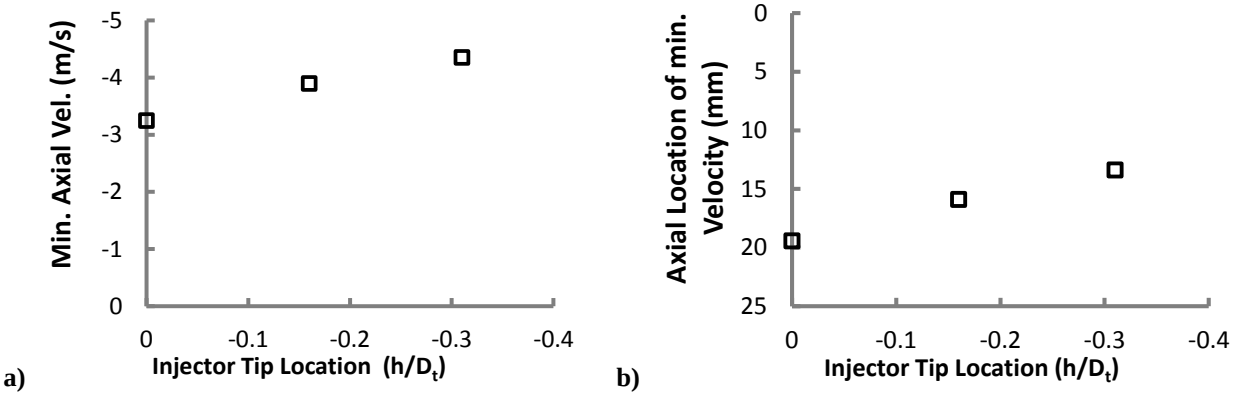

Figure 18. Measures of Strength of Recirculation for 60º Swirler. *a) Plot of minimum axial velocity and b) axial location of minimum velocity versus injector tip location. Test condition 500.*

injector tip is shown in Fig 17 b). The location shows a shifting of the maximum width downstream as the injector tip proceeds downstream, which reflects a simple shifting of the flow downstream.

The minimum axial velocity of the recirculation zone was also measured and is shown in Fig. 18. Figure 18 a) shows that the minimum axial velocity increases as the injector tip is moved further upstream the throat. This trend shows that the location of the injector tip may have an effect on the flow structure when a recirculation zone is present. The location of this maximum reverse flow is shown in Fig. 18 b) plotted against the location of the injector tip. This plot shows a shifting of the maximum velocity downstream as the injector tip is moved downstream.

IV. Summary

The swirler angle has a large effect on the spray angle and the formation of a recirculation zone as shown in Refs. [15], [19] and [20]. The larger the swirler angle the wider the spray angle and the more likely the formation of the recirculation zone. Recirculation only occurred for swirl number S = 1.02, corresponding to the 60° swirler. The injector tip location appears to only shift the flow without changing the structure for most flows. For flows with a recirculation zone, the droplets became more uniform in size and angular distribution the closer the injector tip was to the venturi throat. This relationship between injector tip location and recirculation zone was also shown by considering the minimum axial velocity. The minimum axial velocity increases as the injector tip was moved upstream towards the venturi throat.

Acknowledgments

This work was supported by the Supersonics and Aeronautical Sciences Projects of the NASA Fundamental Aeronautics Program. We also thank Aimee Bogner, Derek Podboy, and Kurt Rusmisel for their technical support.

References

[1] Lee, D.S., Pitari, G.,Grewe, V., Grierens, V., Penner, J. E., Petzold, A., Prather M. J., Schumann, U., Bais, A., Berntsen, T., Iachetti, D., Lim, L. L., and Sausen, R., "Atmospheric Environment", Vol.44 , pp. 4678–4734, 2010.

[2] Tacina, R. R.. "Low-NOx potential of gas turbine engines," AIAA-1989-0550, 1989.

[3] Chang, C. T. and Holdeman, J. D., "Low emissions RQL flametube combustor test results," NASA/TM–2001-211107, 2001.

[4] Peterson, C. O., Sowa, W. A., and Samuelson, G. S., "Performance of a model rich burn–quick mix–lean burn combustor at elevated temperature and pressure," NASA/CR–2002-21192, 2002.

[5] Lee, C. M., Bianco, J., Deur, J. M., and Ghorashi, B., "Nitric oxide formation in a lean premixed prevaporized Jet A/air flame tube: an experimental and analytical study," NASA/TM–2001-105722, 1992.

[6] Tacina, R., Lee, P., and Wey, C., "A lean-direct-injection combustor using a 9 point swirl-venturi fuel injector," ISABE-2005-1106, 2005.

[7] Tacina, R., Mao, C.-P., and Wey, C., "Experimental investigation of a multiplex fuel injector module with discrete jet swirlers for low emissions combustors," AIAA-2004-0135, 2004.

[8] Tacina, R., Wey, C., Laing, P., and Mansour, A., "A low-NOx lean-direct injection,multipoint integrated module combustor concept for advanced aircraft gas turbines," NASA/TM–2002-211347, 2005.

[9] Bianco, J., "NASA Lewis Research Center's combustor test facilities and capabilities," AIAA-1995-2681, 1995.

[10] Lefebvre, A. H. *Gas Turbine Combustion*, 2nd ed., Taylor and Francis, Philadelphia, 1998.

[11] Beer, J. M. and Chigier, N. A. *Combustion Aerodynamics*, 1st ed., John Wiley & Sons, Inc., New York, 1972.

[12] IDL, Exelis Visual Information Solutions, Software Package, Ver. 8.3, Boulder, Colorado, 2013.

[13] Feature.pro, John C. Crocker and David G. Grier, Emory University, Atlanta, Ga, 1996.

[14] Gupta, A.K., Lilley, D.G., and Syred, N., *Swirl Flows*, Abacus Press, Kent, UK, 1984.

[15] Fu, Y., "Aerodynamics and Combustion of Axial Swirlers,", Ph.D. Dissertation, University of Cincinnati, 2008.

[16] Ajmani, K., Mongia, H.C., and Lee, P., "Evaluation of CFD Best Practices for Combustor Design: Part I – Non-Reacting Flows," AIAA 2013-1144, 2013.

[17] Hicks Y. R., Heath, C. M., Anderson, R. C., and Tacina, K. M. "Investigations of a combustor using a 9-point swirl-venturi fuel injector: recent experimental results," ISABE-2011-1106, 2011.

[18] Alekseenko, S.V., Kuibin, P. A., Okulov, V. L., *Theory of Concentrated Vortices*, Springer-Verlag, Berlin, 2007.

[19] Kilik, E, "The Influence of swirler design parameters on the aerodynamics of the downstream recirculation region". Ph. D. Dissertation, School of Mechanical Engineering, Cranfield Institute of Technology, 1976.

[20]Bafuwa, G. G. and Maccalum, N. R. L, "Turbulent Swirling Flames Issueing from vane Swirlers", 18th Meeting of Aerodynamics Panel, I.F.R.F. 1970.